

Architecting the Ground Segment of an Optical Space Communication Network

Iñigo del Portillo, Marc Sanchez, Bruce Cameron, Edward Crawley
Massachusetts Institute of Technology
77 Massachusetts Ave 33-409
Cambridge, MA 02139
{portillo,msnet,bcameron,crawley}@mit.edu

Abstract—Optical communications are envisioned as a key technology for space communication in the near future. This transition to optical terminals is being pushed by the higher data volume demand of certain missions (i.e.: missions DESDyNI (now cancelled) and NISAR had together a requirement of 60 Tb/day, whereas the data-volume transmitted daily by the Space Network nowadays is roughly 40 Tb) and by the spectrum encroachment in current RF bands. In addition, recent missions like LLCD and OPALS have demonstrated that optical systems present multiple advantages with respect to RF terminals, such as their lower mass, size and power and the higher data-rate they offer (up to 10 Gbps). However, one of the main issues of using optical systems is the space-to-ground link, due to the difficulty of penetrating through atmospheric clouds. Geographic diversity of ground stations has been proposed as an alternative to mitigate these effects. The goal of this paper is to analyze different architectures for the ground segment of a fully optical space relay-communications network to serve LEO missions. In particular, we analyze the tradespace characterized by the decisions 1) number and location of optical ground stations, 2) use of GEO relay satellites vs. direct to Earth (DTE) approach and 3) presence of crosslinks among relay satellites.

To that end, we use historical NOAA’s weather data and the cloud fraction dataset from Aqua’s and Terra’s MODIS instruments to characterize weather conditions across the globe. We later use these models to determine the best locations to place ground stations that support optical terminals. Next, we present ONGSA, a network simulator that incorporates the cloud models in order to simulate end-to-end operations of the optical network. Finally we exercise ONGSA to explore the aforementioned tradespace and analyze both cost and performance (in terms of availability) for each architecture.

TABLE OF CONTENTS

1. INTRODUCTION.....	1
2. OPTICAL NETWORK GROUND SEGMENT ANALYZER.....	2
3. TRADESPACE DESCRIPTION AND OPTIMIZATION ..	7
4. RESULTS	8
5. CONCLUSIONS.....	10
ACKNOWLEDGMENTS	12
REFERENCES	12
BIOGRAPHY	13

1. INTRODUCTION

Motivation

Optical communications are envisioned as a disruptive technology for space communications in the near future. Dif-

ferent authors have proposed hybrid RF-optical networks using both space and ground based assets, in which optical technology is proposed as a substitute for RF equipment for inter-satellite links (ISL) and space-to-ground links (SGL). [1]

This transition to optical terminals in the space-industry is being pushed by higher data volume demands of missions forecasted in the 2040 horizon (i.e. missions DESDyNI and NISAR had together a down-link requirement of 60 Tb/day, whereas the data-volume transmitted daily by the space network (SN) nowadays is roughly 40 Tb) and by the spectrum encroachment in current RF bands. In addition several studies [2],[3] show that optical systems outperform traditional RF communication systems in terms of weight, size, power and data-rate. Finally, the last demonstrations of free-space optical (FSO) communications systems show that we are at a point where the TRL and cost associated with FSO technology is high enough to consider it viable for operational deployment and start architecting networks that will replace current RF-based systems.

One of the main challenges of switching from RF SGL to optical SGL is ensuring network availability in the presence of clouds. As the optical beam cannot penetrate clouds, link disruption occurs in the event of covered sky over the receiving ground stations. A solution proposed to mitigate weather outage is site diversity of the receiver stations. In this way, if a satellite locks onto an optical ground station (OGS) and during its transmission a cloud blocks the link it can switch to another OGS and continue downloading its data to Earth. Thus, site diversity increases the network availability.

The improvement on availability highly depends on the number and location of the ground stations. A network with a very high number of OGS might achieve an excellent performance in terms of availability, but at the same time it might result in exorbitant maintenance costs that render the system unaffordable. Therefore, a compromise between performance and cost must be achieved when determining the location of the ground stations.

Literature Review

Previous works have studied the problem of mitigating cloud effect through site diversity both from a simulation and an analytical perspective. Most of the studies analyze the network reliability in terms of availability, which in turn is defined as the fraction of time such that at least one Cloud-Free Line of Sight (CFLOS) path exists between a satellite and a ground station.

References [4] and [5] exercise the Lasercom Network Optimization Tool (LNOT), a proprietary software simulation tool that uses a high resolution cloud database constructed using NOAA’s GOES satellite imagery to determine the fraction of

978-1-4799-5380-6/15/\$31.00 2015 IEEE.

¹ IEEEAC Paper #2574, Version 1, Updated 21/10/2015.

time that a CFLOS is available to the a deep space probe. Both publications limit the number of possible locations to a list of facilities and frame the optimization problem as downselecting the subset of N OGS that maximizes the network availability. Candidate locations in [4] are all within the US territory whereas in [5] the list of possible locations is extended with stations located all across the globe. [6] is a preceding study of these documents where authors analyze the effect of site diversity for an optical network that communicates with the (later scrapped) Mars Laser Communications Demonstration. They include in their analysis other factors that contribute to link outage such as aerosol attenuation, sky radiance and atmospheric seeing. [7] is a comprehensive report based on LNOT that includes single point analysis for 6 different scenarios (LEO, HEO, GEO, L1, L2 and Deep Space).

Reference [8] builds its cloud dataset from ISCCP [9] and also uses a simulation approach to analyze the network availability for an Earth Observation LEO satellite. However, the authors do not perform optimization over the design space for the locations of the OGS in the network, but analyze a particular configuration.

On the other hand, reference [10] proposes an analytical model to quantify the probability distribution for the network availability, both assuming a binary attenuation channel where cloud coverage causes link disruption and assuming a continuous model where clouds introduce an attenuation over the signal that depends on their thickness.

This literature review highlights two main aspects relevant for the OGS network architecting process and that previous work lack. First, most of the existing publications are devoted to analyze the availability of a network whose users are deep space probes. Second, none of the papers develop cost models to analyze the trade-off between performance and cost. Finally, even though models based on simulation are more accurate than analytical ones, they are computationally expensive and therefore unsuitable for performing system architecture studies.

Paper Structure

The remainder of this paper is organized as follows: Section 2 presents the Optical Network Ground Segment Analyzer (ONGSA), a computational tool to assess the cost and availability of a particular OGS network. In particular, we present the assumptions and hypothesis that are the basis of the cloud model, the procedure to compute the network availability given an scenario and a set of OGS and the cost model used by the tool. Next, section 3 describes the scenarios considered in this study together with the optimization algorithm used to explore the space of possible ground segment architectures. In turn, section 4 presents the results of exercising ONGSA and looking at different trade-offs that appear on the architectural design space. Lastly, Section 5 derives conclusions from the research and outlines the future directions of research in this area.

2. OPTICAL NETWORK GROUND SEGMENT ANALYZER

The goal of this section is to provide an overview of the Optical Network Ground Segment Analyzer Tool, the architectural tool developed to analyze the availability and cost of an optical space communication network. The tool is capable of enumerating thousands of ground segment architectures,

evaluate them and explore the design space using a Multi-Objective Genetic Algorithm. Moreover, the network can compute the Network Availability (NA) in three different scenarios: customer missions in LEO downlinking data to the ground segment through geostationary relay satellites with ISL among them, customer missions downlinking information through geostationary relay satellites without ISL and customer missions downloading information directly to the OGS through Direct to Earth (DTE) links.

We start this section describing how the cloud model was built. Next, we present the other two main components of the tool, the Availability Assessment Module and the Cost Model Module.

Cloud model

There are many different cloud models of varying complexity on the literature. Some of them use low level data from satellites, satellite imagery and registers from weather stations combined with physical models, whereas others come in a more statistical flavor and aggregate all this low level data into a single equation. The former are generally more accurate but require a higher computational power to predict the cloud behavior, whereas the latter are less precise but their outputs can be easily stored and evaluated much faster.

As execution speed on the evaluation of our architectures is a desirable property when doing tradespace exploration, we discard physical models and opt for using a statistical framework for our cloud model. This model is based on NASA's Earth Observations Cloud Fraction dataset [11],[12], a L3 data product which represents the fraction of time a certain location has a cloudy sky. The data is projected onto the Climate Modeling Grid with a grid-resolution of 0.10° both in latitude and longitude. The cloud fraction data is available in a daily, weekly and monthly basis since the year 2000 for both satellites Terra and Aqua. Figure 1 shows the cloud fraction over the globe for the month of August 2015.

Our model characterizes every possible latitude/longitude location with a certain probability of cloud for every month ($\theta_{i,j,m}$, with $i = \text{lat}$, $j = \text{lon}$ and $m = \text{month}$). In other words, we have a Bernuilli distributed random variable for every possible location. We approximate θ as the average value of the cloud fraction value for both satellites Terra and Aqua. We use monthly values for $\theta_{i,j,m}$ as there are seasonal correlations (both positive and negative) among diverse locations that we want our model to capture. For example, if we had a ground segment architecture were all the OGS are located in the north hemisphere, it might happen that the performance of the network decreased substantially during the months of November-February (winter in the northern hemisphere). This effect could be easily mitigated by selecting OGS in both hemispheres.

An important parameter to compute the network availability, as we will see in the next section is the Link Outage Probability (LOP). This is defined as the probability that all the OGS that are in LOS with a satellite fail due to cloud coverage at the same time. Note that if the ground stations are assumed to be independent, the probability of this happening can be computed as the product of individual probabilities:

$$\text{LOP}_P = \prod_{g \in G} \theta_{g_L, g_l} \quad (1)$$

where G is the set of ground stations in line of sight (LOS) from point P g_L and g_l denote the latitude and longitude of

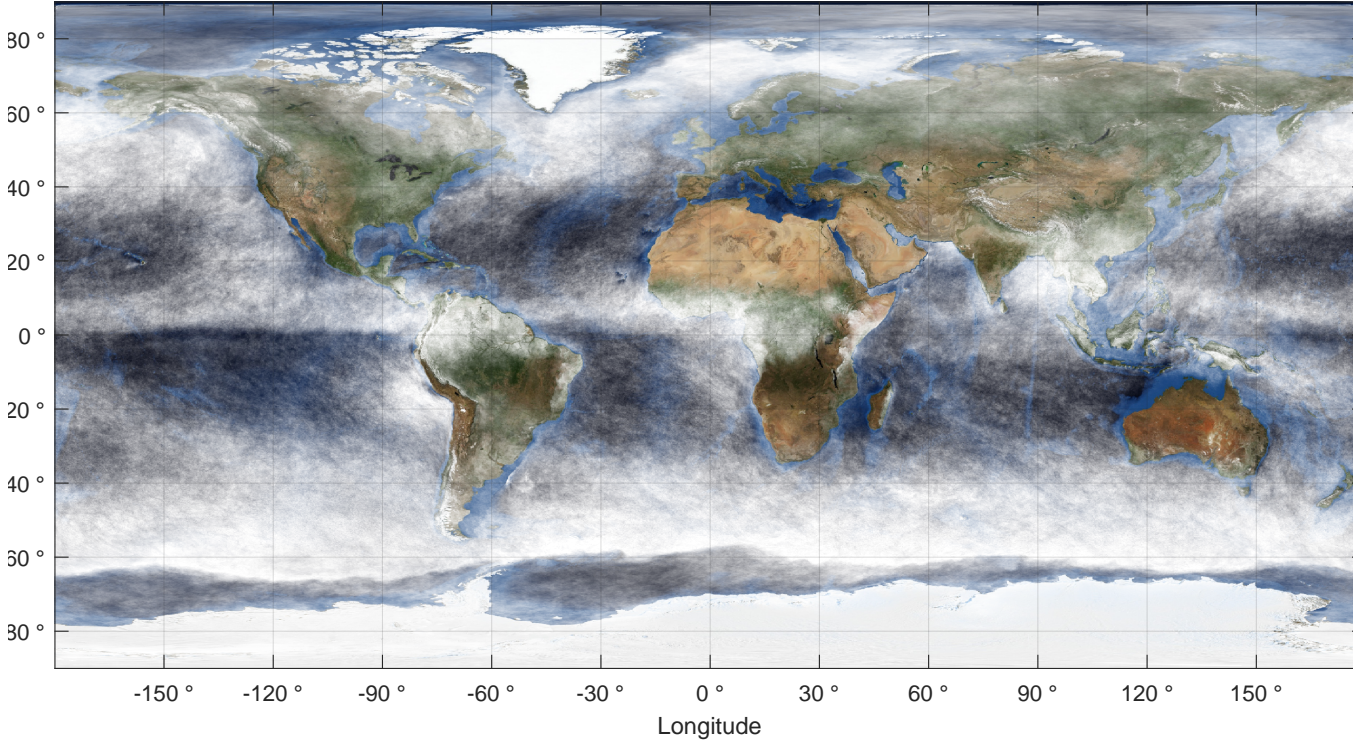


Figure 1: Average cloud fraction for the month of August 2015. White shaded areas represent a cloud probability close to 1.

ground station g respectively. This is the approach followed by references [8], [13]. However, the premise of statistical independence is not valid when the distance between ground stations falls below a certain threshold [14], as weather conditions are tightly correlated in spatially close locations.

Assuming statistical independence when in reality the ground stations are correlated can yield to erroneous results, as described in [10]. To avoid this, we need to include the effect of cloud correlation in our calculations. In [10] the authors propose sampling-based techniques to simulate the real behavior of the correlated random processes. However, these techniques are computationally too expensive for architectural studies, as the LOP for each architecture must be computed thousands of times, drawing different cloud probability values every-time.

A more computationally affordable procedure is described in [14], where spatial distribution of clouds is characterized analytically by fitting an exponential model to real data gathered every 6 hours for 5 years in 33 different locations in Spain. In particular, they describe the statistical dependence index as the ratio between the real joint probability $\mathbf{P}(\mathbf{A} \cap \mathbf{B})$ and the product of the marginal probabilities $\mathbf{P}(\mathbf{A})$, $\mathbf{P}(\mathbf{B})$, as shown in Eq. 2.

$$\mathbf{P}(\mathbf{A} \cap \mathbf{B}) = \chi_{\mathbf{A},\mathbf{B}}\mathbf{P}(\mathbf{A})\mathbf{P}(\mathbf{B}) \quad (2)$$

where \mathbf{A} and \mathbf{B} refer to the events “Clouds over the OGS_x ”, $x \in \{\mathbf{A}, \mathbf{B}\}$ and $\chi_{\mathbf{A},\mathbf{B}}$ is the statistical dependence index.

As our model extends to the whole globe, we replicate the results from [14] using a dataset of 4,000 sites in the US, South America, Australia, Europe and Southeastern Asia. This data was downloaded from NOAA’s National Climatic Data Center (NNDC) DS3505 dataset which contains infor-

mation of the cloud coverage status every 20 minutes.

Cloud coverage information in NNDC is represented by the number of oktas of the sky which are covered. We pre-process the bulk data in order to remove those ground stations with insufficient values or those whose registers are not reliable. Next, we compute the values for $\mathbf{P}(\mathbf{A} \cap \mathbf{B})$, $\mathbf{P}(\mathbf{A})$, $\mathbf{P}(\mathbf{B})$ and $\chi_{\mathbf{A},\mathbf{B}}$ for every pair of ground stations and we adjust an exponential model to the data using the distance, latitude and longitude of each of the ground stations as independent variables. None of the coefficients were significant apart from the distance between ground stations. Eq. 3 presents the resulting model whereas Fig. 2 shows how the adjusted model fits the data points.

$$\begin{aligned} \chi_{\mathbf{A},\mathbf{B}} &= \alpha_0 + \alpha_1 \exp\left(-\frac{d}{d_0}\right) = \quad (3) \\ &= 0.98 + 0.71 \exp\left(-\frac{d}{424.1}\right) \end{aligned}$$

We note that our model presents a slightly higher cloud correlation distance (d_0 in Eq. 3) than the one provided in the model derived in [14].

The cloud model described has several limitations that need additional considerations. First, only architectures where ground stations are at most pairwise spatially correlated can be evaluated. We limit ourselves to these situations (by filtering out those architectures that do not satisfy this constraint) in the analyses we present in section 4. Second, our model does not capture other temporal correlations apart from the seasonal correlation. This includes for examples correlations due to day-night effects or jet-stream effects. even though we believe that most of the cases these represent second order effects, when looking at the statistical “tails” corresponding

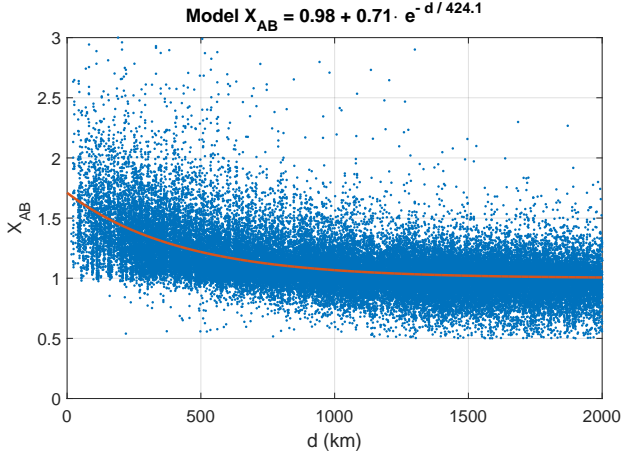


Figure 2: Statistical dependence index ($\chi_{A,B}$) against distance between a pair of Ground Stations.

to very high availabilities they might dominate. Quantifying the effect of these correlations when looking at the will be addressed in future work. Finally, note that the real value of the statistical dependence index shows a high dispersion with respect to its fitted model. This is due to the difficulty of such a simple exponential regression model to fit all the different correlation situations between close ground stations. The root mean-square deviation of the value of $\chi_{A,B}$ is 0.2.

Availability Assesment Module

As our cloud model is discretized in time using months as the time unit, we start by defining the monthly Network Availability (NA_m). The monthly Network Availability is the probability of a satellite in a random orbit having at least one ground station in Cloud-Free Line of Sight (CFLOS) at any point in time of month m . The monthly Link Outage Probability (LOP_m) is defined as the complement of the monthly Network Availability (NA_m) as denoted in Eq. 4. Finally, we define the Network Availability (NA) as the percentile 95 of the time series of monthly Network Availabilities.

$$NA_m = 1 - LOP_m \quad (4)$$

In order to compute the availability of a given network of OGS, we use the following 4 step procedure.

First, we compute for each optical ground station (OGS_i) a mask (M_{gs_i}) that indicates which points at a given height (h) will be in line of sight with the ground station. For that purpose, we define a 1° resolution (both in latitude and longitude) spherical grid with radius $R_E + h$ (R_E is the radius of the Earth) and compute the set of points of the grid whose elevation angle is above the minimum elevation angle admissible at the receiver ground station. The elevation angle between a point of the grid (P) and a particular OGS can be computed using Eq. 6, 6

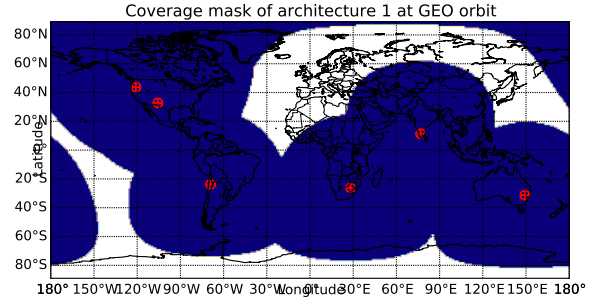
$$M_{gs_i} = \{P = (L_P, l_P) | \epsilon(P) > \epsilon_{min}\} \quad (5)$$

$$\epsilon(P) = \arccos \frac{\sin \gamma}{\sqrt{1 + \frac{R_E^2}{R_E+h} - 2 \frac{R_E}{R_E+h} \cos \gamma}}$$

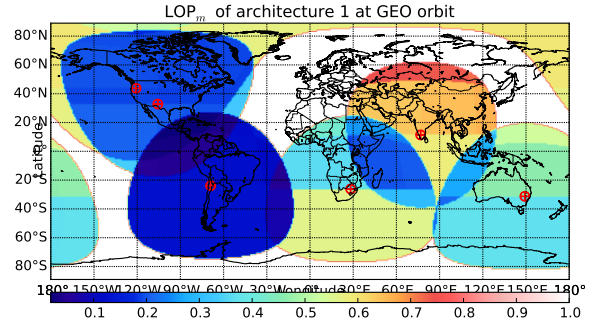
$$\cos(\gamma) = \sin L_P \sin L_{OGS} + \cos L_P \cos L_{OGS} \cos(l_P - l_{OGS}) \quad (6)$$

where L_{OGS} and l_{OGS} are respectively the latitude and longitude coordinates of the OGS, L_P and l_P are the latitude

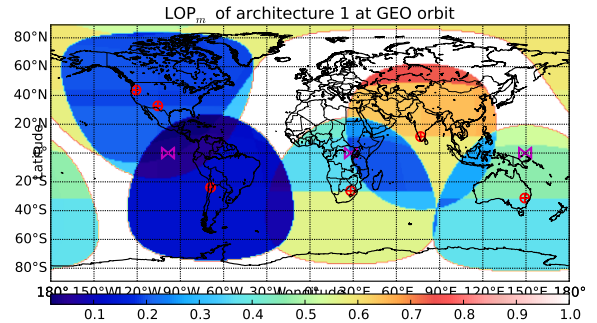
and longitude coordinates of the point i of the spherical grid, h is the height at which the spherical grid is located and ϵ_{min} is the minimum elevation angle in order to achieve a successful communication. In this work we assume $\epsilon_{min} =$



(a) Step 1 - Determine the coverage mask at GEO



(b) Step 2 - Determine the LOP_m for each point of GEO



(c) Step 3 - Deterrmine the Location of the satellites (marked in purple)

Figure 3: Procedure to compute NA_m

Second, we determine the LOP_P for each point of the mask by computing on which point will the optical beam pierce the cloud layer (estimated being at a height of 12 km.). In addition, some orbits are more popular than others, so the probability of a satellite being in LOS with a OGS is not uniform among all points of the mask. In order to account for this effect, we determine the satellite density over the Earth surface, that is, over which points lat/lon of the Earth's

surface is more likely to find a satellite with its Nadir point toward that point.

For that purpose we create an STK² scenario with all the active satellites in LEO whose mission belongs to one of the following categories: Scientific, Earth Observation, Weather, Human Space Flight or Technology Demonstrator. Then we propagate their orbits and register their lat/lon coordinates (discretized to a 0.1 degree resolution) for a period of a year with a 10 second time-step. Finally we determine the probability of having a satellite whose nadir intersects every point of the globe using a frequentist approach. We denote the 3600×1800 matrix with the probability of having a satellite over point P as $D(P)$. This results are plotted in Fig. 4.

Third, if our scenario has relay satellites, we determine their optimal location. In our scenarios, we assume that we have a set of 3 satellites in GEO that relay the communications of the LEO satellites to/from an OGS. This system is similar to TDRSS [15] configuration. However, we assume that the orbital slots where the relay satellites are located are not pre-defined but optimized for every OGS network architecture.

Finding the optimal slots for the relay satellites can be formulated as a mathematical optimization problem described by Eq. 7.

$$L^*(s_i) = \arg \max_{L(s_i)} \text{Per}_{95} [\text{NA}(L(S), \text{OGS})_m] \quad (7)$$

s.t.

$$110 \leq |L(s_i) - L(s_j)| \leq 130 \quad \forall i, j, \quad i \neq j$$

$$L(s_i) \in [-180, 180]$$

where $\text{Per}_{95}[\cdot]$ stands for the percentile 95%, $L(s_i)$ denotes the orbital slot of the relay satellite i , and $\text{NA}(L(S), \text{OGS})_m$ is a function that computes the monthly Network Availability at month m given the location of the satellites and the set of OGS that compose the architecture. Note that the first constraint enforces that satellites are evenly spaced in the geostationary orbit.

In this study we consider two forms for the availability function $\text{NA}(L(S), \text{OGS})$ depending whether the relay satellites have cross-link capabilities or not.

Results of steps 1-3 for a test architecture with OGS in Chile, Australia, India, the Canary Islands and the USA can be observed in Figure 3.

Fourth, once the optimal location of the relay satellites has been determined, we proceed to compute the actual NA for the architecture. The next subsections described how the NA is computed for different scenarios.

Availability for GEO relay satellites—As we have said, we define the Network Availability as $\text{NA} = \text{Per}_{95}[\text{NA}_m]$. The monthly Network Availability (NA_m) can be computed from the monthly Link Outage Probability (LOP_m), as by Eq. 4 one is the complement of the other. So let's start by defining how to compute the LOP_m at a certain point P .

Let the set $\{\text{OGS}_P\}$ be the set of ground stations in direct visibility with a satellite located in point P and $C(\text{gs})$ be the event it is cloudy over the optical ground station gs for $\text{gs} \in \text{OGS}_P$. Then, the probability that the satellite cannot

communicate back with any of the OGS is given by:

$$\text{LOP}_{P,m} = P \left(\bigcap_{i=1}^N C(\text{gs}_i) \right) \quad \forall \text{gs} \in \text{gs}_P \quad (8)$$

We can compute $P(\bigcap_{i=1}^N C(\text{gs}_i))$ as the product of the individual $P(C(\text{gs}_i))$ for those ground stations that are statistically independent to all the other OGS in the network and according to Eq. 2 as $\chi_{i,j} P(C(\text{gs}_i)) P(C(\text{gs}_j))$ for those who are spatially correlated. It's easy to see that this formulation derives erroneous results if more than 2 ground stations are correlated, as we only considers pairwise correlations. To avoid mistakes, the tool ensures on its ground station selection procedure (previous to the availability computation) that no more than two ground stations will be correlated in a valid architecture.

Now, if we focus on the scenario in which we have 3 relay satellites that can communicate amongst them using their cross-links, then the monthly Network LOP is equal to the probability that none of the relay satellites can communicate with any of the ground stations they are in line of sight with. The NA_m is then the complement of the product of the individual LOPs for each satellite s_i , $i = \{1, 2, 3\}$

$$\text{NA}(L(S), \text{OGS})_m = 1 - \prod_{i=1}^3 \text{LOP}_{L(s_i),m} \quad (9)$$

where $L(s_i)$ refers to the point in space where satellite i is located.

On the other hand, if the relay satellites do not possess ISL, then we compute NA_m using the following procedure:

1. For each satellite s_i compute a mask that determines which points of a sphere with radius $R_E + 600\text{km}$ (the sphere that contains the LEO with $h = 600\text{ km}$) are in his LOS.
2. Compute the availability as described in Eq. 10

$$\text{NA}(L(S), \text{OGS})_m = \left(1 - \sum_{p \in M_{s_i}} D(p) \text{LOP}_{L(s_i),m} \right) \quad (10)$$

Availability for LEO satellites using Direct to Earth downlink—Another plausible scenario for optical communications is one where satellites down-link their data directly to the OGS. In this case the network monthly LOP can be computed by simply multiplying the LOP for each point of the sphere with radius equal to $R_E + 600\text{km}$ (the sphere that contains all the possible circular orbits with height 600 km) by the satellite density matrix $D(p)$ and aggregating over all the possible points p . The monthly NA is its complement as described in Eq. 11.

$$\text{NA}(L(S), \text{OGS})_m = \left(1 - \sum_{p \in P} D(p) \text{LOP}_{p,m} \right) \quad (11)$$

where p denotes one point of the grid, $D(\cdot)$ is the satellite density matrix and LOP_p is the link outage probability of point p .

²AGI's Systems ToolKit <http://www.agi.com/products/stk/>

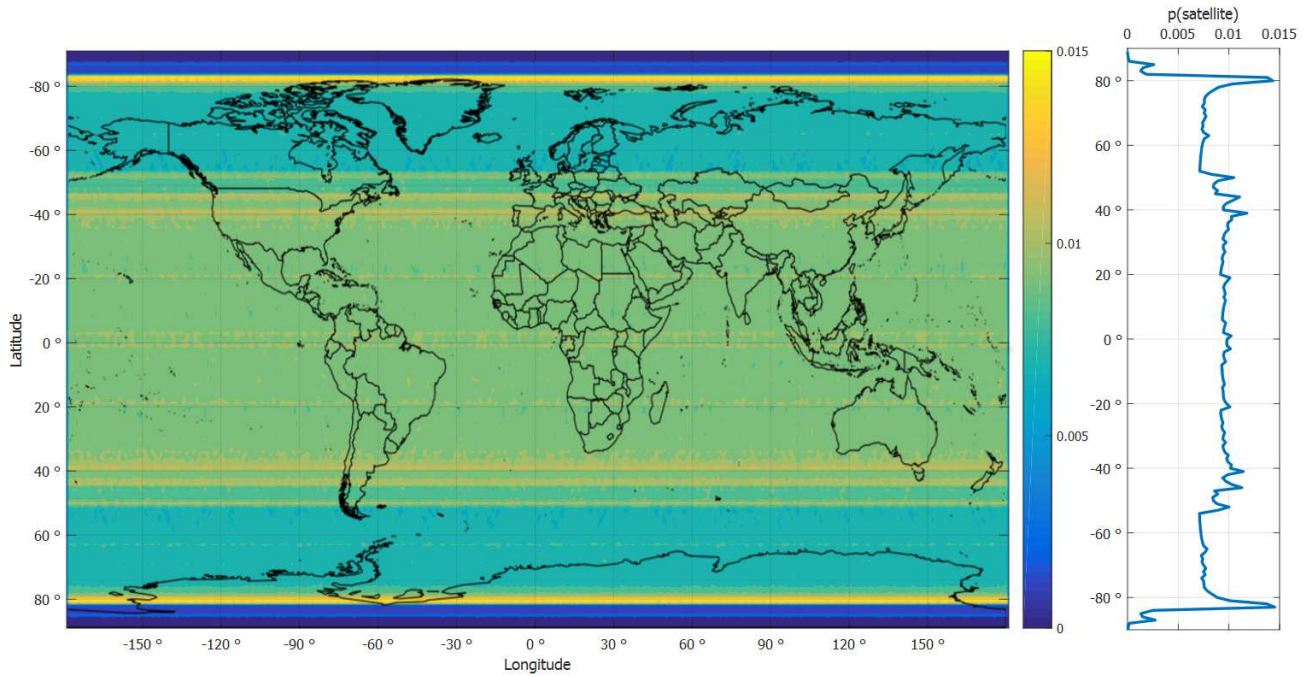


Figure 4: Satellite density over the surface of Earth. Note that there is only a dependence with the latitude.

Cost model

The goal of the cost model module is to come up with an estimation of the lifecycle cost of a ground segment architecture that is good enough for relative comparison across architectures. The cost of an architecture is the sum of the costs of each of the OGS that compose it. At the same time, the OGS cost is split into non-recurring investment costs and recurring operational costs. The drivers of the recurring costs are employees salary, wide area communication operational costs and reparation and maintenance of the facility.

In this section we describe the equations to estimate the costs for each of these components. All the monetary values in this section are in FY2015\$k.

Non recurring cost—The main drivers of the non-recurring cost are site construction, optical terminal cost, and wide area communication network development. This costs are only incurred once, when the ground station is built. This subsection describes the parametric model for each of the aforementioned costs.

Estimating the cost of a single optical terminal has been analyzed in references [16], [17], [18], [19]. The vast majority of the existing models relates the cost of a telescope to a single variable, its diameter, whereas some authors in the literature [19] present multivariate cost models that include other parameters such as the year of development, TRL, or the number of segments.

For monolithic telescopes, most references provide a model where the cost is proportional to the diameter of the telescope to the power of 2.6 ([20], [16]) or 2.7 ([21], [17]). In this work we assume a similar model and adjust the coefficients using the data points included in the Optical Link Study Group Final Report [7]. The values of the CERs used in the model are presented in Eq. 12. This model is valid for

small telescopes with a diameter smaller than 1.5 m, which is always the case in our analysis.

$$C_{tels} = 6,230 \text{ \$k } D_{tel}^{2.7} \quad \text{if } D_{tel} \leq 1.5m \quad (12)$$

On the other hand, the site construction cost is estimated using a parametric model from the DoD Facilities Pricing Guide [22]. The model uses a unit cost per square meter ($\$/m^2$) for each type of facility which is multiplied by a) the dimensions of the facility and b) the *area cost factor* which accounts for differences in labor, material and equipment in different geographic locations.

$$C_{cons} = F(L) \cdot U_c \cdot A_{gs} \quad (13)$$

where $F(L)$ is the area cost factor, U_c is the unit construction cost and A_{gs} are the dimensions of the facility (estimated to be $1780 m^2$).

Finally, the WAN communication investment is modeled to be proportional to the distance from the ground station to the closest Internet eXchange Point (IXP). This way we intend to capture the cost associated to establishing a high-bandwidth wide area network cable to the ground station. The CER for the WAN cost is presented in Eq. 14, where the value of 15.9 k\$ is obtained as the higher cost of the fiber optic cable installation estimated for the year 2013 by the U.S. Department of Transportation [23] :

$$C_{WAN,nr} = 15.9k\$ \cdot d_{IXP} \quad (14)$$

where d_{IXP} is the distance to the closest IXP. The locations of the IXP across the globe were obtained from the EIEA³ database that contains 513 entries.

³European Internet Exchange Association <https://www.euro-ix.net/>

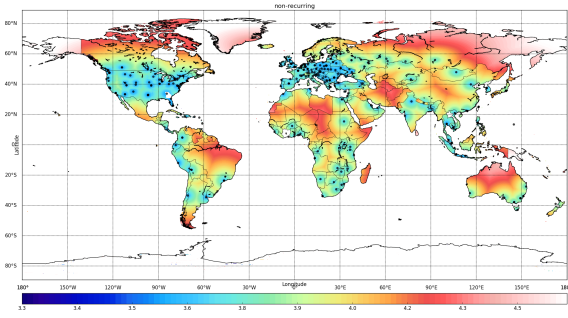


Figure 5: World-map of non-recurring cost (in M\$, FY2015) for a new OGS. Black markers denote the position of an IXP.

All in all, the construction cost is computed as:

$$C_{nr} = F(L)(C_{WAN,nr} + C_{cons} + C_{tels}) \quad (15)$$

where $F(L)$ is the cost area factor for a ground station located in country L . Figure 5 presents a world-map with the non-recurring cost for each lat/lon point.

Recurring cost—Our cost model assesses the recurring cost of a ground station as the sum of three different components: employees salary, operational costs of the WAN and maintenance and operational cost of the facility and the telescope.

First, we estimate that each OGS employs 3 qualified engineers plus 10 local employees for maintenance and operational tasks. The salary of the former is estimated to be 80 \$k/year while the latter's salary is 1.6 times the average wage of the country where the OGS is located. Average wages for each country were collected from the CIA World Factbook [24]. Therefore, the total expense in salaries per year in a ground station is:

$$C_{salary} = 10 \cdot 1.6 \cdot W(L) + 3 \cdot 80 \frac{\text{k\$}}{\text{year}} \quad (16)$$

where $W(L)$ is the average wage in country L .

Second, the WAN operational cost ($C_{WAN,r}$) is estimated to be 390 k\$ per year, as described in [25]. Finally, the maintenance and operational costs are given by the sustainment cost (as described in [22]) multiplied by the sustainment cost factor (which again depends on the country the facility is located on) and the dimensions of the facility.

$$C_{M\&O} = S(L) \cdot U_s \cdot A_{gs} \quad (17)$$

where $S(L)$ is the sustainment cost factor in country L , U_s is the unit sustainment cost and A_{gs} are the dimensions of the facility.

All the terms in the non-recurring cost are multiplied by the *inflation factor* as prescribed in [22], which accounts for the future-year inflation/escalation costs for operations and maintenance. In turn, the total recurring cost (C_r) is given by Eq. 18

$$C_r = \sum_{t=1}^T \frac{C_{salary} + C_{WAN,r} + C_{M\&O}}{(1 + I(r))^t} \quad (18)$$

where $I(r)$ is the inflation factor, T is the lifetime of the ground stations (set to 30 years in our analysis) and t is an index that designates the difference between the year in which we are accounting the recurring costs and the initial year (2015).

3. TRADESPACE DESCRIPTION AND OPTIMIZATION

Tradespace Description

Two different approaches have been proposed to make the transition from RF architectures to hybrid RF-optical systems. The first one envisions the existence of geostationary satellites that relay the information sent from the LEO customers to the OGS. This system would imitate the behavior of the SN nowadays. Moreover, the use of optical ISL between the relay satellites has been proposed as an additional mechanism to combat the effects of cloud weather on link disruption.

The second approach for this transition is to develop a system that is similar in its operations to the NEN, that is, the customer missions in LEO download their data directly to the OGS. This approach is easier to carry out, as deploying optical terminals into existing infrastructure entails less risk than deploying optical terminals in space.

In order to understand the implications in terms of availability and cost involve on each of the aforementioned approaches, we define the following three scenarios to serve as inputs for the tool.

- **Scenario A - GEO + ISL:** Customer missions send their data to the optical ground stations through a constellation of 3 relay satellites in GEO that are interconnected through ISL.
- **Scenario B - GEO no ISL:** Customer missions send their data to the optical ground stations through a constellation of 3 relay satellites in GEO that do not dispose of ISL.
- **Scenario C - DTE:** Customer missions send their data directly to the optical ground stations.

Problem Formulation and Tradespace Optimization

Once that we have defined the tradespaces that we want to study, we need to translate our problem into a mathematical formulation. Ideally, we would like to solve an unconstrained optimization problem over the entire surface of Earth, that is, find the best locations to place new OGS (or use existing infrastructure) so that we achieve a certain value of NA at the minimum cost. However, the complexity of this problem makes it intractable from a computational perspective.

In order to reduce the complexity of the optimization, we consider a set of possible locations for the optical ground stations. Each architecture is comprised from a subset of these OGS. Initially we considered 241 candidate locations, but this would yield a design space of $2^{241} \approx 10^{71}$ possible architectures, which in turn makes the problem unsolvable in a reasonable computational time too. Therefore we reduced our listed of candidates by imposing that the OGS must be situated at a minimum height above the sea level of 1000 m. following the guidelines of Chapter 9 in [26]. After applying this criterion our list of possible locations was reduced to a total of 40 element. These are plotted in Fig. 6. Table 3 contains further information on the characteristics of these ground stations.

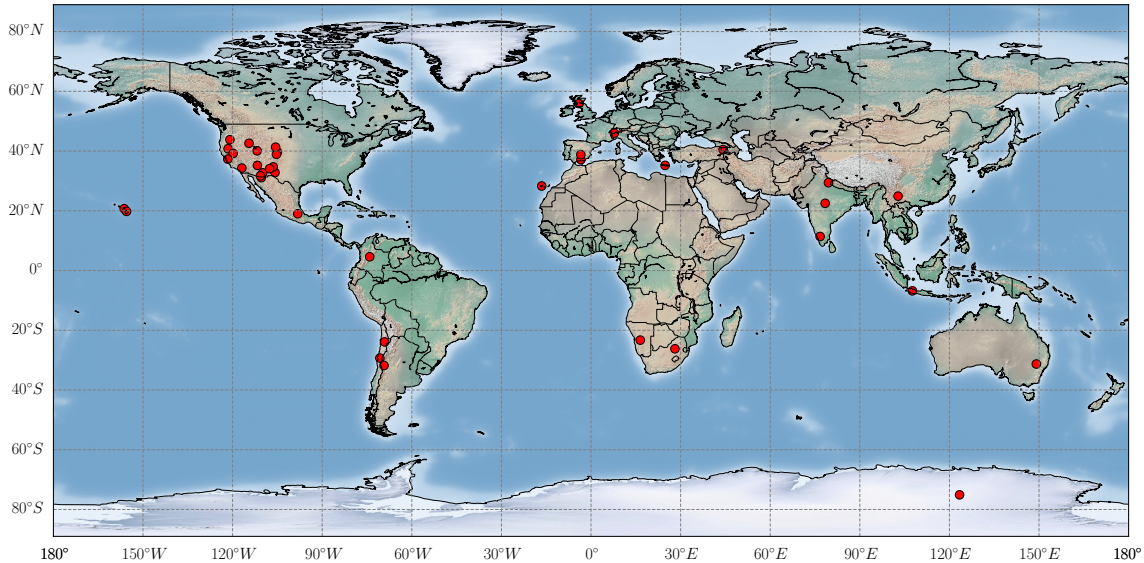


Figure 6: Location of the possible OGS (red markers). A detailed description of the sites can be found in Table 3.

Thus, we can frame our problem as a down-selecting problem [27] where we have to choose a subset of k OGS out of the N candidates locations so that the value (NA at a certain cost) delivered by our network is maximized. This yields to a total number of architectures equal to $\sum_{k=1}^N \binom{N}{k}$. In order to speed up the optimization process and obtain reasonable architectures, we add a constraint by setting the maximum number of OGS in any architecture to 20. This gives us a tradespace with a total of $1.1 \cdot 10^{12}$ different architectures.

This number is still too big to perform a full factorial evaluation. Thus, we have to turn to heuristic techniques in order to solve our problem. ONGSA uses a Genetic Algorithm (GA), a population-based meta-heuristic optimization algorithm to look for the solutions in the Pareto Front. The GA we have implemented follows the prescriptions of the Non-dominated Sorting Genetic Algorithm-II (NSGA-II) a Multi-objective Genetic Algorithm [28].

A NSGA-II operates as follows: Initially, a random population of N architectures is generated and evaluated. Next, $\frac{N}{2}$ architectures are selected to act as parents for the following generation using the following criteria [28]:

- Architectures with lower Pareto ranking are selected first.
- Among architectures with similar Pareto ranking those with lower crowding distance are selected first.

Then, two genetic operators are applied over the selected parent to produce $\frac{N}{2}$ offspring. Our tool implements two genetic operators, *crossover* and *mutation*.

Crossover acts first, and it takes as inputs two parents selected at random (the father and the mother) and produces two offspring (the son and the daughter). In our particular scenario, each architecture is represented using a 40 length bit-string (b), where $b[i] = 1$ means that the i -th OGS is part of the architecture. We use uniform crossover ([29]) over the two bit-strings representing the father and the mother architectures. In uniform crossover initially the son takes his bits from the father and the daughter takes them from her mother. Then, every bit is swapped between son and daughter

with probability 0.5. In total, applying crossover to a set of $\frac{N}{2}$ parents produces $\frac{N}{2}$ new offspring, which conform a new generation of N architectures.

Mutation is a genetic operator that is applied with probability p_{mut} to all the parents and offspring produced by crossover. If mutation is applied to an architecture, we remove an OGS from it with probability p_{remove} . Then, independently of the outcome of this first step, we add a new OGS with probability p_{add} .

After both operators have been applied, we have a new generation to be evaluated again. The process repeats until a termination criterion (i.e. maximum number of generations G_{max} evaluated, no new architectures in the Pareto Front) is met. Our set up of parameters for our GA is $N = 10,000$, $G_{max} = 20$, $p_{mut} = 1$, $p_{add} = p_{remove} = 0.5$.

4. RESULTS

Figures 7, 8 and 9 show the resulting tradespace for scenarios A, B and C respectively after the GA has run for 10 generations. Each dot represents an architecture evaluated. The set of non-dominated architectures is plotted with a thicker edge-line whereas each point's filling color denotes the number of ground station in the architecture. Note that the abscissa axis' range is different on each plot.

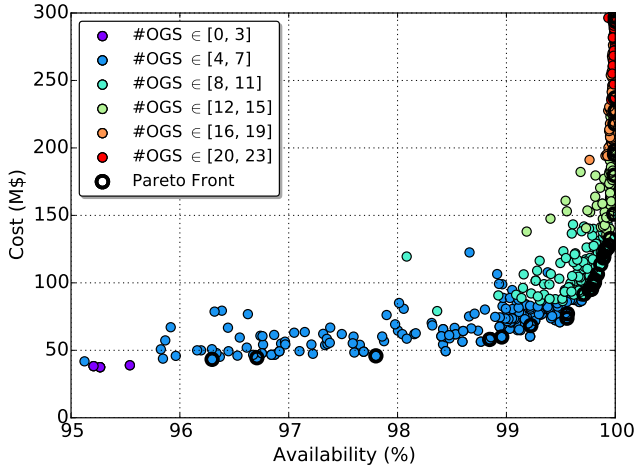


Figure 7: Tradespace of top performing architectures of the Scenario A. Availabilities above 99.9% are achieved with 10 OGS

Figure 7 shows that when using ISL among the relay satellites, very high NA values can be achieved at a reasonable cost. This is due to the positive effect of ISL between the relay satellites, which creates an extra layer to combat the link outage caused by cloud coverage in addition to site diversity. In particular, availabilities of 99.6% can be achieved at a cost slightly smaller than 100 \$M using 7 GS whereas availabilities of 99.99% are achieved at an expense of 180 \$M and 13 OGS. All the configurations in the Pareto share a common pattern in terms on how OGS are selected. These architectures trend to concentrate a high number of OGS in certain regions (most of the times America or the India-Australian region) and place a relay satellite on top of them (in general the stations only serve to this satellite). Then, this satellite is used as the main sink for all the traffic of the network, receiving the traffic from the other satellites through the ISL that connects them.

This design-strategy seems a reasonable choice given how the NA is computed. Besides, concentrating all the OGS in a small region might help to reduce the cost of the terrestrial optical back-haul communications network even though the monetary quantification of this effect is out of the scope of this paper.

Figure 8 displays that using a constellation of 3 relay satellites without ISL guarantees availabilities of 80% at a cost of 100 \$M using 7 GS whereas availabilities of 90.2% are achieved at an expense of 180 \$M and 12 OGS. This results reveal the importance of using ISL on the relay constellation. With a similar number of ground stations and cost we are capable of achieving consistently significant improvements in terms of network availability. If we analyze the design paradigm underlying the optimal architectures, we observe that this is substantially different to the one in optimal architecture of Scenario A; in Scenario B OGS trend to be equally distributed among the whole globe, trying to construct a global robust and reliable ground segment. This spread nature of the network might result as consequence higher costs for the terrestrial back-haul network connecting the OGS, even though this effect is not considered in this paper. Finally, in this scenario, an OGS usually has more than one satellite in LOS, as this contributes to reduce the LOP of both of them.

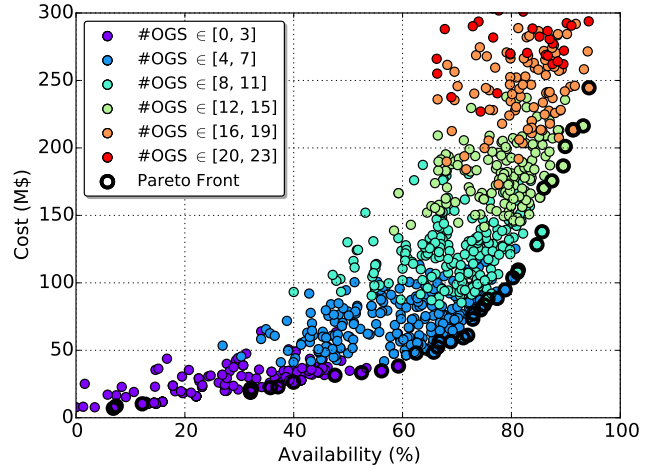


Figure 8: Tradespace of the Scenario B. The maximum availability achieved is 94.6% with 20 OGS

Figure 9 illustrates the behavior of the network when the users download their data using DTE links to the ground stations. We observe that, in comparison with the other scenarios, architectures have a very low score in the NA metric. However, we need to interpret this results carefully as the NA metric is upper-bounded by the global coverage that the network can provide. In that sense, as 71% of the Earth's surface is covered by water and because the antenna mask at a height of 600km is relatively small, the maximum availability achievable (by having a OGS on every piece of continental land) is approximately 29%. As an example, the current configuration of the NEN would score very poorly (5% availability).

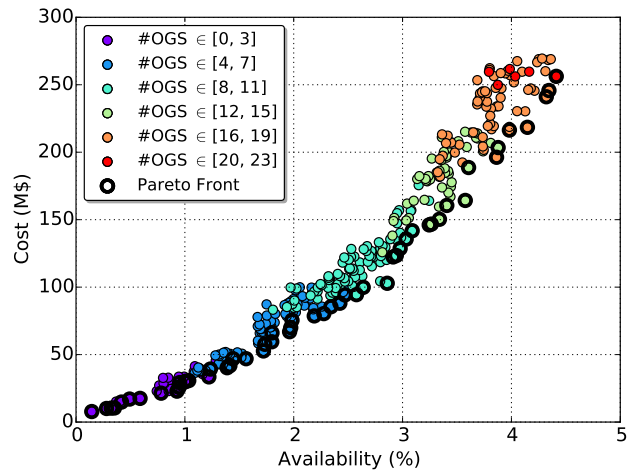


Figure 9: Tradespace of the Scenario C. The maximum availability achieved is 4.57 % with 20 OGS

Finally, Figure 10 presents in the same graphic the Pareto Fronts of the three scenarios for comparison purposes. In this picture the number of ground stations is represented by the opacity of the dots (the more transparent a point, the less ground stations.)

Table 1: Most Popular OGS for different scenarios

Scenario A - GEO + ISL			Scenario B - GEO no ISL			Scenario C - DTE		
Name	#	%	Name	#	%	Name	#	%
La Silla Observatory	34	97.1	High Energy Stereoscopic System	20	74.1	La Silla Observatory	29	59.2
High Energy Stereoscopic System	27	77.1	Aryabhata Research	19	70.4	Aryabhata Research	28	57.1
Aryabhata Research	22	62.9	Ooty Radio Telescope	14	51.9	Observatorio Astronomico	22	44.9
Mount Graham	16	45.7	La Silla Observatory	12	44.4	Felix Aguilar Observatory	21	42.9
Felix Aguilar Observatory	13	37.1	Siding Spring Observatory	9	33.3	High Energy Stereoscopic System	21	42.9
Byurakan Observatory	12	34.3	Bosscha Observatory	8	29.6	IRAM 30m telescope	17	34.7
Atacama Desert	12	34.3	Skinakas Observatory	8	29.6	Skinakas Observatory	16	32.7

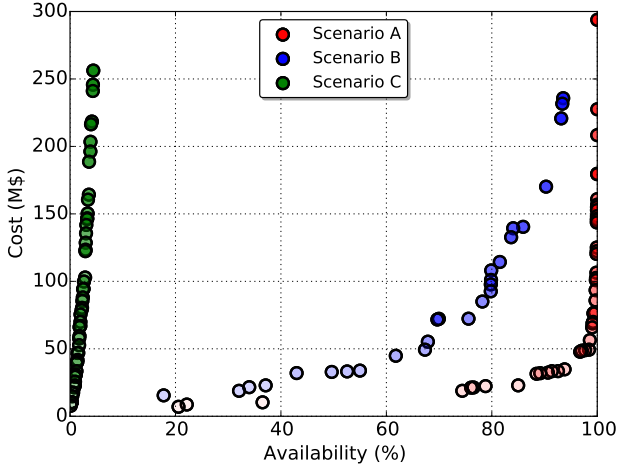


Figure 10: Comparison of the Pareto Fronts for the three Scenarios. The opacity denotes the number of ground stations.

We finish this section by analyzing which OGS are the most and least popular among non-dominated architectures in all three scenarios. Table 1 shows the most popular Pareto front optical ground stations while Table 2 shows the least popular ones. It can be observed that some facilities appear consistently in the Pareto Front for the three different scenarios. This is the case of La Silla Observatory in Chile and Aryabhata Research in India and the High Energy Stereoscopic System in Namibia. Similarly, other stations such as the Large Millimeter Telescope in Mexico, the Very Large Array in New Mexico and the Sierra Nevada Observatory in Spain rarely belong to the non-dominated configurations.

5. CONCLUSIONS

This paper presents a computational tool to assess the performance and cost of a network of OGS for space communications. The tool is composed of three main modules, a cloud model, a network availability evaluator and a parametric cost model. The cloud model has been developed by using MODIS' cloud fraction dataset, expanded with a ground station correlation model derived from data from NOAA's AWOS. The network availability is evaluated by computing the LOP on any point of a spherical grid that contains the set of possible orbits of the transmitter satellites. Finally, the cost model has been built using data from the DoD. As it is envisioned that the optical network has to support communications with a bandwidth of tenths of Gigabits per

second, distance to an Internet eXchange Point is one of the main drivers of the cost of the system.

In order to demonstrate the usefulness of the tool a tradespace study has been conducted. In this study three scenarios that analyze the main architectural decisions for the ground segment have been considered. We have formulated the problem of selecting the best locations as a combinatorial optimization problem and a Genetic Algorithm has been proposed as a heuristic method to solve this problem. The optimization has been conducted among a reduced set of possible location consisting of current ground stations, mainly composed of astronomical observatories.

Finally, results show that some OGS are systematically selected in the set of non-dominated architectures. In addition, our analysis shows that using a constellation of relay satellites results in a considerable increase for the Network Availability. Finally, achieving NA values similar to those obtained by TDRSS (above 99%) at a reasonable cost requires the use of ISL between relay satellites. This has been proven to be a cost effective solution that adds an extra mitigation layer to combat the effect of cloud coverage. In particular, having ISL results in an increase from 80% of availability with 7 GS at a cost of 100 \$M to 99.6 % of availability with the same number of ground stations and a similar cost.

Future Work

The main stream of research for future is the study of the unconstrained problem for the location of the OGS. That is, instead of restricting the possible locations of the ground stations to a set of sites around the globe, allow the optimizer to choose any point on the land surface of the Earth. We believe that current astronomical observatories were not designed to act as high bandwidth elements in a global network, but just attending to low cloud coverage probabilities and high altitude criteria. Even though those are clearly desirable attributes for an OGS, their faraway locations might result in extra cost for the WAN investment and maintenance. In that sense, allowing new locations for the OGS might yield to surprising results.

In addition, we are working to include a more accurate model for the optical link budget that allows us to 1) have better estimates of the dimensions of the telescopes and 2) understand how second order effects affect to the NA. In particular we are working in a model than uses the height above sea level of the OGS as well as the atmospheric refractive index in order to evaluate the LOP caused by second order factors such as scintillation and phase distortion effects.

Table 2: Least Popular OGS for different scenarios

Scenario A - GEO + ISL			Scenario B - GEO no ISL			Scenario C - DTE		
Name	#	%	Name	#	%	Name	#	%
James Clerk Maxwell Telescope	0	0	Sierra Nevada Observatory	0	0	Hat Creek Radio Observatory	0	0
Yunnan Astronomical Observatory	0	0	Teide Observatory	0	0	Sierra Nevada Observatory	0	0
Red Buttes Observatory	0	0	Large Millimeter Telescope	0	0	Haleakala Observatory	1	2.9
Sierra Nevada Observatory	0	0	Dome C	0	0	Large Millimeter Telescope	1	2.9
Herrett Observatory	0	0	James Clerk Maxwell Telescope	1	2.9	Very Large Array	1	2.9
Large Millimeter Telescope	0	0	Hat Creek Radio Observatory	1	2.9	Jack C. Davis Observatory	1	2.9
Very Large Array	0	0	Herrett Observatory	1	2.9	Guillermo Haro Observatory	2	5.7

Table 3: List of Possible Locations for the OGS

Name	Latitude	Longitude	Altitude (m)	City / State	Country
Airdrie Public Observatory	55.9	-4.0	1085.0	Airdrie	Scotland
Apache Point Observatory	32.8	-105.8	2791.6	New Mexico	USA
Aryabhata Research Institute of Observational Sciences	29.4	79.5	1932.0	Uttarakhand	India
Atacama Desert Observatory	-23.9	-69.1	2641.7	Antofagasta	Chile
Big Bear Lake Solar Observatory	34.3	-116.9	2057.3	Big Bear City	California
Bosscha Observatory	-6.8	107.6	1304.9	West Java	Indonesia
Byurakan Observatory	40.5	44.2	4058.8	Mount Aragats	Armenia
Capilla Peak Observatory	34.7	-106.4	2837.6	New Mexico	USA
Chamberlin Observatory	39.7	-105.0	1643.1	Denver	USA
Dome C	-75.1	123.4	3265.0	-	Antartica
Felix Aguilar Observatory	-31.8	-69.3	2420.5	San Juan	Argentina
Guillermo Haro Observatory	31.1	-110.4	2477.3	Sonora	Mexico
Haleakala Observatory	20.7	-156.3	3025.5	Hawaii	USA
Hartebeesthoek Radio Astronomy Observatory	-26.2	28.1	1723.5	Gauteng	South Africa
Hat Creek Radio Observatory	40.8	-121.5	1018.9	Shasta County	USA
Herrett Observatory	42.6	-114.5	1138.2	Twin Falls	USA
High Energy Stereoscopic System	-23.3	16.5	1826.7	Khomas Region	Namibia
IRAM 30m Telescope	37.1	-3.4	3364.5	Pico Veleta	Spain
Jack C. Davis Observatory	39.2	-119.8	1426.8	Carson City	USA
James Clerk Maxwell Telescope	19.8	-155.5	4197.3	Mauna Kea	USA
KOSMA Observatory	46.0	7.8	3109.7	Gornergrat	Switzerland
La Silla Observatory	-29.3	-70.7	2331.1	Coquimbo	Chile
Large Millimeter Telescope	19.0	-98.2	2144.0	Puebla	Mexico
Las Brisas Observatory	38.9	-105.3	2615.8	Colorado	USA
Lick Observatory	37.3	-121.6	1285.4	Mount Hamilton	USA
Lowell Observatory	35.2	-111.7	2204.9	Arizona	USA
Mount Graham	32.7	-109.9	3259.3	Arizona	USA
Observatorio Astronomico Nacional	4.6	-74.1	2555.0	Bogota	Colombia
Ooty Radio Telescope	11.4	76.7	2249.1	Tamil Nadu	India
Pachmarhi Array of Cerenkov Telescopes (PACT)	22.5	78.4	1065.7	Madhya Pradesh	India
Pine Mountain Observatory	43.8	-120.9	1908.8	Oregon	USA
Red Buttes Observatory	41.3	-105.6	2184.1	Wyoming	USA
Siding Spring Observatory	-31.3	149.1	1134.7	New South Wales	Australia
Sierra Nevada Observatory	38.8	-3.4	2034.7	Sierra Nevada	Spain
Skinakas Observatory	35.2	24.8	1585.3	Crete	Greece
Teide Observatory	28.3	-16.5	2386.1	Canary Islands	Spain
Very Large Array	34.1	-107.6	2123.6	Socorro	USA
West Mountain Observatory	40.1	-111.8	1385.7	Utah	USA
Winer Observatory	31.7	-110.7	1488.8	Sonoita	USA
Yunnan Astronomical Observatory	24.9	102.8	1929.9	Yunnan	China

APPENDIX

Acronyms

CER	Cost Estimating Relationship
CFLOS	Cloud-Free Line of Sight
DESDyNI	Deformation Ecosystem Structure and Dynamics of Ice
DSN	Deep Space Network
DoD	Department of Defense
FSO	Free Space Optics
FY	Fiscal year
GA	Genetic Algorithm
GEO	Geosynchronous Orbit
GOES	Geostationary Operational Environmental Satellites
GRTG	Guam Remote Ground Terminal
GSFC	Goddard Space Flight Center
ISL	Intersatellite Link
ISS	International Space Station
IXP	Internet eXchange Point
LEO	Low Earth Orbit
LCRD	Laser Communications Relay Demonstration
LLCD	Lunar Laser Communication Demonstration
LNOT	Laser network Optimization Tool
LOP	Link Outage Probability
LOS	Line of Sight
MIT	Massachusetts Institute of Technology
NA	Network Availability
NA _m	Monthly Network Availability
NASA	National Aeronautics and Space Administration
NEN	Near Earth Network
NISAR	NASA-ISRO Synthetic Aperture Radar
NNDC	National Climatic Data Center
NOAA	National Oceanic and Atmospheric Administration
NSGA-II	Non-Dominated Sorting Genetic Algorithm - II
OGS	Optical Ground Station
ONGSA	Optical network Ground Segment Analyzer
SCaN	Space Communication and Navigation
SGL	Space to Ground Link
SN	Space Network
STK	Systems ToolKit
TDRSS	Tracking and Data Relay Satellite System
TRL	Technology readiness level
WAN	Wide Area Network

ACKNOWLEDGMENTS

The authors would like to thank the *Fundación Obra Social de La Caixa* for partially funding this project.

REFERENCES

- [1] V. W. Chan, "Free-space optical communications," *Lightwave Technology, Journal of*, vol. 24, no. 12, pp. 4750–4762, 2006.
- [2] A. K. Majumdar, *Advanced Free Space Optics (FSO): A Systems Approach*. Springer, 2014, vol. 186.
- [3] H. Henniger and O. Wilfert, "An introduction to free-space optical communications," *Radioengineering*, vol. 19, no. 2, pp. 203–212, 2010.
- [4] R. Link, M. E. Craddock, and R. J. Alliss, "Mitigating the impact of clouds on optical communications," in *Aerospace Conference, 2005 IEEE*. IEEE, 2005, pp. 1258–1265.
- [5] G. S. Wojcik, H. L. Szymczak, R. J. Alliss, R. P. Link, M. E. Craddock, and M. L. Mason, "Deep-space to ground laser communications in a cloudy world," in *Optics & Photonics 2005*. International Society for Optics and Photonics, 2005, pp. 589 203–589 203.
- [6] A. Biswas, K. E. Wilson, S. Piazzolla, J. P. Wu, and W. H. Farr, "Deep-space optical communications link availability and data volume," in *Lasers and Applications in Science and Engineering*. International Society for Optics and Photonics, 2004, pp. 175–183.
- [7] O. L. S. Group, "Optical link study group final report," Interagency Operations Advisory Group, Tech. Rep., June 2012.
- [8] D. Giggenbach, F. Moll, C. Fuchs, and M. Brechtelsbauer, "Direct optical high speed downlinks and ground station networks for small LEO missions," in *16th Ka- and Broadband communications conference*, 2010.
- [9] W. B. Rossow and R. A. Schiffer, "ISCCP cloud data products," *Bulletin of the American Meteorological Society*, vol. 72, no. 1, pp. 2–20, 1991.
- [10] N. Perlot and J. Perdigues-Armengol, "Model-oriented availability analysis of optical GEO-ground links," in *SPIE LASE*. International Society for Optics and Photonics, 2012, pp. 82 460P–82 460P.
- [11] Platnick, S., Ackerman, S., King, M., et al., "MODIS Atmosphere L2 Cloud Product (06L2)," *NASA MODIS Adaptive Processing System, Goddard Space Flight Center*, 2015.
- [12] EOS Project Science Office. Nasa earth observations - cloud fraction.
- [13] N. Perlot and F. Moll, "Probability distributions of link durations with n disruptive channels: application to ground-space optical communications," in *SPIE Optical Engineering+ Applications*. International Society for Optics and Photonics, 2012, pp. 851 710–851 710.
- [14] P. Garcia, A. Benarroch, and J. M. Riera, "Spatial distribution of cloud cover," *International Journal of Satellite Communications and Networking*, vol. 26, no. 2, pp. 141–155, 2008.
- [15] J. Teles, M. Samii, and C. Doll, "Overview of TDRSS," *Advances in Space Research*, vol. 16, no. 12, pp. 67–76, 1995.
- [16] T. Schmidt-Kaler and P. Rucks, "Telescope costs and cost reduction," in *Optical Telescopes of Today and Tomorrow*. International Society for Optics and Photonics, 1997, pp. 635–640.
- [17] L. M. Stepp, L. G. Daggert, and P. E. Gillett, "Estimating the cost of extremely large telescopes," in *Astro-*

nomical Telescopes and Instrumentation. International Society for Optics and Photonics, 2003, pp. 309–321.

- [18] M. R. Garcia-Talavera, C. Rivera, G. Murga, I. Montilla, and A. Alonso, “Analysis of large optical ground stations for deep-space optical communications,” in *International Conference on Space Optics*, vol. 7, 2014, p. 10.
- [19] H. P. Stahl, G. Holmes Rowell, G. Reese, and A. Byberg, “Multivariable parametric cost model for ground-based telescopes,” vol. 5497, 2004, pp. 173–180. [Online]. Available: <http://dx.doi.org/10.1117/12.552167>
- [20] J. Lesh and D. Robinson, “A cost-performance model for ground-based optical communications receiving telescopes,” *TDA Progress Report 42*, vol. 87, pp. 56–64, 1986.
- [21] P. Y. Bely, “Large space optics,” in *Next Generation Space Telescope Science and Technology*, vol. 207, 2000, p. 25.
- [22] Department of Defense. (2015) The DoD Facilities Pricing Guide.
- [23] Office of the Assistant Secretary for Research and Technology, U.S. Department of Transportation. Unit cost entries for fiber optic cable installation. [Online]. Available: <http://www.itscosts.its.dot.gov/its/benecost.nsf/DisplayRUCByUnitCostElementUnadjusted?ReadForm&UnitCostElement=Fiber+Optic+Cable+Installation+&Subsystem=Roadside+Telecommunications>
- [24] D. C. I. A. Washington. (2013) The world factbook 2013-14.
- [25] K. Schulz, J. Rush *et al.*, “Optical link study group final report,” *IOAG-15b*, June, 2012.
- [26] H. Hemmati, *Near-earth laser communications*. CRC Press, 2009.
- [27] D. Selva, “Rule-based system architecting of earth observation satellite systems,” Ph.D. dissertation, Massachusetts Institute of Technology Department of Aeronautics and Astronautics, Cambridge, Massachusetts, June 2012.
- [28] K. Deb, A. Pratap, S. Agarwal, and T. Meyarivan, “A fast and elitist multiobjective genetic algorithm: NSGA-II,” *Evolutionary Computation, IEEE Transactions on*, vol. 6, no. 2, pp. 182–197, 2002.
- [29] G. Syswerda, “Uniform crossover in genetic algorithms,” 1989.

BIOGRAPHY



Barcelona.

Inigo del Portillo is a graduate student in the department of Aeronautics and Astronautics at MIT. His research interests include optical communications for space-based networks and small satellites communications. Inigo received his degrees in Industrial Engineering, Electronics Engineering and Telecommunications Engineering in 2014 from Universitat Politècnica de Catalunya,



Marc Sanchez Net is currently a second year M.S. student in the department of Aeronautics and Astronautics at MIT. His research interests include machine learning algorithms and rule-based expert systems, and their suitability to the fields of system engineering and space communication networks. Prior to his work at MIT, Marc interned at Sener Ingeniería y Sistemas as a part of the team that develops and maintains FORAN, a CAD/CAM/CAE commercial software for shipbuilding. Marc received his degrees in both Industrial engineering and Telecommunications engineering in 2012 from Universitat Politècnica de Catalunya, Barcelona.



Dr. Bruce Cameron is a Lecturer in Engineering Systems at MIT and a consultant on platform strategies. At MIT, Dr. Cameron ran the MIT Commonality study, a 16 firm investigation of platforming returns. Dr. Cameron’s current clients include Fortune 500 firms in high tech, aerospace, transportation, and consumer goods. Prior to MIT, Bruce worked as an engagement manager at a management consultancy and as a system engineer at MDA Space Systems, and has built hardware currently in orbit. Dr. Cameron received his undergraduate degree from the University of Toronto, and graduate degrees from MIT.



Dr. Edward F. Crawley received an Sc.D. in Aerospace Structures from MIT in 1981. His early research interests centered on structural dynamics, aeroelasticity, and the development of actively controlled and intelligent structures. Recently, Dr. Crawley’s research has focused on the domain of the architecture and design of complex systems. From 1996 to 2003 he served as the Department Head of Aeronautics and Astronautics at MIT, leading the strategic realignment of the department. Dr. Crawley is a Fellow of the AIAA and the Royal Aeronautical Society (UK), and is a member of three national academies of engineering. He is the author of numerous journal publications in the *AIAA Journal*, the *ASME Journal*, the *Journal of Composite Materials*, and *Acta Astronautica*. He received the NASA Public Service Medal. Recently, Prof. Crawley was one of the ten members of the presidential committee led by Norman Augustine to study the future of human spaceflight in the US.